*Journal of Statistical Physics, Vol. 112, Nos. 1/2, July 2003 (© 2003)*

# On the Lowest Energy Nucleation Path in a Supersaturated Lattice Gas

**Vitaly A. Shneidman**[1]

*Received July 19, 2002; accepted February 6, 2003*

A lattice gas with non-conserved spin flip dynamics (of both non-Glauber and Glauber types) is considered at $T \ll T_c$, the critical temperature. For arbitrary supersaturation, $S$, a general expression for the inverse of the nucleation rate along the lowest energy path is derived. The exponential part is identical to the one by Neves and Schonmann [*Commun. Math. Phys.* **137**:20 (1991)]. The preexponential can be expressed in terms of elliptic theta-functions for small $S$, and in the limits, respectively, of $S \gg T/\phi$ or $S \ll T/\phi$ ($-\phi$ being the nearest-neighbor interaction energy), elementary versions of the general expression are further obtained. The preexponential has a smooth component, as well as small-scale modulations which are approximately periodic in the inverse supersaturation. For $S \ll T/\phi$, the smooth part is proportional to $\sqrt{S}$, in contrast to the zero-$T$ limit where it is linear in $S$. The latter limit becomes apparent only at extremely low temperatures which are cubic in $S$.

**KEY WORDS:** Nucleation; lattice gas; Glauber dynamics; preexponential.

## 1. INTRODUCTION

Metastable states are a common phenomenon in physics, ranging from condensed matter[1–3] to cosmological[4] systems. Nucleation is a typical mechanism for decay of a metastable state via fluctuational formation and growth of nuclei of the stable phase. Developments in nucleation theory deepen one's understanding of the general rules which govern such processes and, potentially, allow one to increase control over metastability in specific applications.

As a rule, for any given metastable system the starting point of a nucleation description is evaluation of the nucleation barrier, $W_*$, as suggested by Gibbs. Once $W_*$ is known, one obtains the exponential part of

[1] Department of Physics, New Jersey Institute of Technology, Newark, New Jersey 07102; e-mail: vitaly@oak.njit.edu



0022-4715/03/0700-0293/0 © 2003 Plenum Publishing Corporation

the nucleation rate, as first shown by Volmer and Weber.[5] Further specification[5] comes with the evaluation of the prefactor to the exponential expression. In some systems, such as glass-forming melts, this prefactor can compete with the exponential term. In most other cases the exponential term is dominant. Nevertheless, it is still the prefactor which distinguishes the fine detail in kinetics of specific systems and without which a theory is incomplete, while comparison with experiment, including simulations, can be ambiguous. One of the best illustrations of the importance and complexity of the prefactor issue could be the "Lothe–Pound paradox"[6] in vapor condensation (for discussion of the paradox see, e.g., ref. 7).

In real systems inevitable inaccuracies in $W_*$ can blur the preexponential, leaving open questions with respect to its absolute values and dependences on temperature and supersaturation. In this context, the interest in Ising-type lattice models stems from the fact that $W_*$ for such systems, and thus the exponential, can be evaluated exactly, allowing one to focus on the more delicate prefactor. The limits where $W_*$ can be obtained include either small supersaturation, $S$, ("field" in magnetic terminology), or small temperature $T$. In the former case the nucleus is macroscopic, and its shape as well as the value of $W_*$ can be determined from the Wulff droplet construction both for the two-dimensional square[8] and the hexagonal[9] lattices. For small $T$, on the other hand, only the lowest energy configurations need to be considered, which simplifies the evaluation of $W_*$.

At higher temperatures non-classical preexponentials were considered in refs. 10–13. Large scale Monte Carlo simulations[14, 15] and numerical transfer matrix methods[16] seem to confirm the theoretical predictions, although such simulations are necessarily restricted to larger supersaturations (to ensure a reasonably moderate $W_*$), and the question of precise identification of the preexponential with any of the classical or non-classical expectations remains open.[17]

In the opposite limit $T \to 0$, the barrier $W_*$ for a square lattice can be obtained for arbitrary field.[18] The nucleus here is composed of a finite number of spins, and does not have to follow the Wulff construction.[19] The preexponential of the nucleation rate at $T = 0$ was considered analytically for Glauber spin-flip dynamics in ref. 20 at large supersaturations. Results pointed towards a discontinuity at a relatively strong field, equivalent to $S = 1/2$ in present notations. Similar discontinuities were later anticipated for Metropolis dynamics in another mathematical study[21] for smaller $S$, again with excluded even integer values of $1/S$. Special values of $S$ were considered in simulations using the technique of Monte Carlo with absorbing Markov chain algorithms.[22, 23]

The case of $T > 0$ and arbitrary, though not too small $S$, was studied analytically (partly, with the use of symbolic computations) in ref. 24 for

another, lattice gas dynamics which is somewhat different from Glauber's, as described in the next section. Sharp peaks were found in the pre-exponential at integer $1/2S = 1$ and $1/2S = 2$. More recently[25] a similar structure of the pre-exponential was observed for Glauber dynamics as well using the aforementioned simulation technique.

The present goal is to study the domain of small $T$ at arbitrary fixed $S$. In a sense, the treatment is complementary to the one in ref. 24 where restrictions on temperature were more relaxed, while $S$ was limited from below by $1/6$. A useful electric analogy will be introduced, which allows one to visualize the nucleation flux as an electric current flowing in a network of variable resistors, and which simplifies calculations. Results will be obtained analytically, without the use of symbolic computations, and both lattice gas and Glauber dynamics will be considered.

The paper has the following structure. In the Background section the model and the basic notations are introduced. The minimal work required to form a cluster of $n$ particles is shown to exhibit two types of maxima as a function of $n$: the primary maxima, which generally determine the barrier $W_*$, identical to the one by Neves and Schonmann,[18] and the secondary maxima which can compete with $W_*$ under special circumstances. The dynamics for particle creation and annihilation is also described in that section.

In Section 3 kinetic equations for evolution of the cluster number densities are presented, starting with the conventional approach[5] (which is valid as long as the nucleation path does not branch), and then generalizing it to include the multiplicity of cluster shapes and branching of paths. An electric analogy (to be used later) is also introduced here.

In Section 4 the pre-exponential is defined, and the limit $T = 0$ is considered. Earlier results are generalized for smaller $S$ for both lattice gas and Glauber dynamics. Much of the required reduction of the "electric network" can be completed at this stage, simplifying further treatment.

In Section 5 results are extrapolated to $T > 0$, giving the upper bound for the preexponential, and asymptotes are evaluated for various relations between $S$ and $T$. Section 6 contains the discussion.

## 2. BACKGROUND AND OUTLOOK

### 2.1. The Model

Consider a standard two-dimensional lattice gas, as described, e.g., in ref. 26. The interaction potential between two particles has a value of $-\phi$ (with a positive constant $\phi$) if particles are nearest neighbors, and is zero

otherwise. For sufficiently large negative values of the chemical potential $\mu$, the lattice gas will represent a dilute mixture of mostly single-particle clusters with a few clusters of larger size.

Let us characterize a *class*—(clusters which can be made identical by rotation, translation or reflection) by a running index $k$, with $k=0$ corresponding to an empty site. The equilibrium number density of such clusters can be written as

$$f_k^{eq} = w_k \exp\{[n(k)\,\mu + \phi b(k)]/T\} \tag{1}$$

with $n(k)$ and $b(k)$ being, respectively, the number of occupied sites ("particles") and nearest-neighbor pairs in a cluster. The integer number $w_i \leqslant 8$ relates to rotational and reflectional symmetry of a cluster, with $w_i = 1$ for a perfect square or an empty site. Equation (1) follows from the grand canonical distribution when interaction between clusters can be neglected—see, e.g., the discussion in ref. 27.

Consider now the chemical potential as the control parameter of the system. For large compact clusters one has for the number of nearest neighbors $b(k) \approx 2n(k)$, excluding the surface effects. Thus, for $\mu < \mu_0 \equiv -2\phi$ the density of large clusters is exponentially small, corresponding to the gas phase. Conversely, for $\mu_0 < \mu < 0$ the lattice gas is metastable and will tend to nucleate the liquid phase once a dynamics is added to the system. Formally, metastability is indicated by the divergence of $f_k^{eq}$ for clusters close to a compact shape with $n(k) \to \infty$; a rather careful definition of "restricted ensembles" is required if one intends to treat the problem rigorously.[28] Physically, the distributions are expected to be close to $f_k^{eq}$ only for cluster smaller than some "critical size" (to be specified below), for which reason distributions $f_k^{eq}$ are often called "quasi equilibrium" in nucleation literature.

Let us define a dimensionless supersaturation

$$S = (\mu - \mu_0)/2\phi \tag{2}$$

The domain of metastability discussed above corresponds to $0 < S < 1$ and will be of the main interest for the present study. Larger $S$ lead to an "unstable" gas where $f_k^{eq}$ looses physical meaning even for a single-particle cluster, since the number of such clusters would exceed the number of empty sites. It turns out, however, that once the kinetic equations are formulated, crossing to $S > 1$ becomes less dramatic (it is just that nucleation, usually associated with crossing of a barrier, will be replaced by a simpler unhindered creation of particles), and formally at least, this region can be considered within the general scheme.

Using a simple geometric relation for the perimeter of a cluster

$$P = 4n - 2b \tag{3}$$

(the argument $k$ will be dropped when no confusion can occur), one can re-write $f_k^{eq}$ in a more familiar form as

$$f_k^{eq} = w_k \exp(-W_k/T) \tag{4}$$

with

$$W_k = \phi(P/2 - 2Sn) \tag{5}$$

being the "work" required to create a cluster of a given class, and $\phi/2$ playing the role of the zero-temperature interfacial tension.

## 2.2. Energies of Cluster Formation

In the low temperature limit of main interest will be compact clusters, with the smallest perimeter $P$ for a given $n$. The easies way to obtain a representative for each $n$ is to start with a single particle and to add subsequent particles in a "spiral." Resulting clusters are always close to rectangular with possibly one incomplete layer. For clusters which are not complete rectangles the perimeter does not change when a particle is added. Otherwise, the perimeter is increased by 2 when a new layer has to be started.

More specifically, if the number of particles $n$ is located between two perfect squares

$$m^2 \leqslant n < (m+1)^2 \tag{6}$$

the perimeter of any compact cluster can have only three possible values

$$P_n = \begin{cases} 4m, & n = m^2 \\ 4m+2, & m^2+1 \leqslant n \leqslant m^2+m \\ 4m+4, & m^2+m+1 \leqslant n < (m+1)^2 \end{cases} \tag{7}$$

The work $W$ thus becomes a piecewise linear function of $n$, as in Fig. 1. There are two types of maxima. The primary maxima ("$p$") correspond to

$$n_p = m^2+m+1, \qquad W_{n_p} = \phi\{2m+2-2Sn_p\} \tag{8}$$

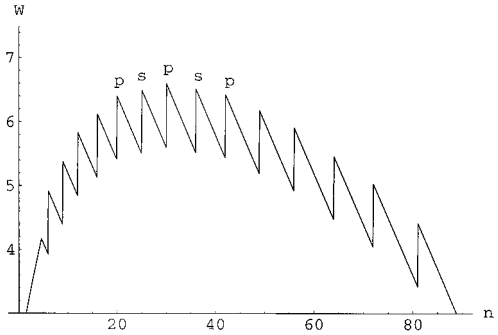


Fig. 1. Reduced "work" $W_n/\phi$ as a function of the number of particles $n$ in a cluster for $S = 0.09$. Note two types of local maxima—the primary at $n = n_p$, Eq. (8), and the secondary at $n = n_s$, Eq. (9). The absolute primary maximum determines the critical size and the barrier to nucleation.

(which is an $m$ by $m+1$ rectangle with one extra particle on the longer side). The secondary ("$s$") maxima are

$$n_s = m^2 + 1, \qquad W_{n_s} = \phi\{2m + 1 - 2Sn_s\} \tag{9}$$

which is a square with one extra particle on any side. In both cases $m$ can be any natural number. These two types of extremal classes will be of the main interest since, under appropriate supersaturation, they can turn "critical," with the corresponding value of $W$ determining the barrier to nucleation.

The critical value of $m$ is given by

$$m_* = [1/2S] - 1 \tag{10}$$

with $[x]$ representing the smallest integer larger than $x$ (note that this definition of $[x]$ differs by 1 from the one used in ref. 24). The number of particles in a critical cluster, $n_*$, and $W_*$—the barrier to nucleation at $T = 0$, are determined by Eq. (8) evaluated for $m = m_*$. Similar expressions for $n_*$ and $W_*$ are well known in mathematical literature.[18] Note, however, that for an integer $1/2S$ two primary and one secondary maximum will have identical values. This will play an important role in the kinetics described below.

## 2.3. Dynamics and Cluster Kinetics

Let new gas particles be allowed to enter the system with a rate $e^{\mu/T}$, i.e., $dt\, e^{\mu/T}$ is the probability for a particle to appear at any empty site

during an infinitesimal interval $dt$. An existing particle disappears with probability $dt \exp(-\phi\, \Delta b/T)$ with $\Delta b \geqslant 0$ being the reduction in the number of nearest neighbors. (A more detailed description of a similar dynamics, as well as references to crystallization applications and Monte Carlo realizations can be found in refs. 17 and 29). To simplify notations, one could rescale time to get a unit rate for injection of particles, with $\exp[-(\mu+\phi\, \Delta b)/T]$ being the rate with which particles disappear.

A cluster from class $i$ can randomly gain a particle and change class to $k$ with $n(k) = n(i)+1$. The probability of this event in a time interval $dt$ is given by $\beta_{i,k}\, dt$, and the gain rate, $\beta_{i,k}$ can have a value 0, 1, 2, 4, or 8, depending on geometry.

The rate of a reverse process—transition to a lower class via loss of a particle—is given by

$$\alpha_{i,k} = \exp\left\{\frac{\phi}{T}\left(\frac{P_k - P_i}{2} - 2S\right)\right\}, \qquad i < k \tag{11}$$

This satisfies detailed balance

$$\beta_{i,k} f_i^{eq} = \alpha_{i,k} f_k^{eq} \tag{12}$$

More complex processes, such as breaking of a cluster into two parts, will have a negligible effect at low temperatures.[30]

## 2.4. Glauber Dynamics

In Glauber dynamics the energies of cluster formation are expected to be identical to those introduced above. The difference comes through the transition rates which are related to those in lattice gas dynamics by

$$\beta_{i,k}^G = \beta_{i,k} \frac{1}{\exp\{(W_k - W_i)/T\} + 1} \tag{13}$$

The loss rates, $\alpha_{i,k}^G$, will not be required since they automatically recovered from detailed balance. Similarities of the correction factor with the one encountered in Fermi statistics are obvious, and indeed under certain assumptions Glauber dynamics can be deduced from a quantum hamiltonian with each spin coupled to a fermionic heat bath.[25, 31]

In the nucleation context, note that the correction factor rapidly oscillates with $n$ between a value close to 1 for a favorable transition with $W_k < W_i$ and an exponentially small value in the opposite case. This adds certain extra features to the Glauber case compared to the lattice gas dynamics where the gain rates $\beta_{i,k}$ change moderately, between 1 and 8.

In Metropolis dynamics (MD) the sum of the two terms in the denominator in Eq. (13) is replaced by their maximum. The MD is identical to the lattice gas dynamics discussed above for "downhill" transitions with $W_k < W_i$ (which are less important for the nucleation problem), and for "idle" transitions with $W_i = W_k$, which are encountered only for $S = 1$ and $S = 1/2$ between the smallest clusters. Otherwise, the MD is asymptotically close to the Glauber dynamics for all transitions with $W_k \neq W_i$, and except for the two aforementioned values of the supersaturation, the nucleation predictions of the two dynamics are expected to be identical at $T \to 0$.

## 3. THE KINETIC EQUATIONS

### 3.1. Conventional Nucleation Kinetics

In the standard approach[5] all clusters ("droplets") are assumed to have similar shapes and can be characterized by a single parameter $n$, the number of particles (which, in the present context can also be identified with the class index, $k$). Nucleation is then treated as a one-dimensional random walk in the $n$-space. The master equation for the kinetic distribution of clusters $f_n$ with fluxes $j_n$ can be written as

$$\frac{df_n}{dt} = j_n - j_{n+1}, \qquad j_n = \beta_{n-1,n} f_{n-1} - \alpha_{n-1,n} f_n \tag{14}$$

With the neglect of depletion of small clusters (which happens on exponentially large time scales), the left-hand boundary condition can be taken as $f_0 = 1$, similarly to refs. 5. The right-hand boundary condition is taken as $f_n \to 0$ for $n \to \infty$.

Equations (14) are usually referred to as the "Becker–Döring" equations, although various closing conditions are often implied (see the analysis in ref. 32). For $f_0 \equiv 1$, a steady-state distribution, $f_n^{st}$, will be established which corresponds to an $n$-independent flux with a value $I$ being the "nucleation rate." Detailed balance allows to exclude one group of kinetic coefficients in Eq. (14), leading to a recurrence relation $f_n^{st}/f_n^{eq} = f_{n+1}^{st}/f_{n+1}^{eq} + I/(\beta_{n,n+1} f_n^{eq})$. With the aforementioned right-hand boundary condition this gives $f_n^{st}/f_n^{eq} = I(1/\beta_{n,n+1} f_n^{eq} + 1/\beta_{n+1,n+2} f_{n+1}^{eq} + \cdots)$. From the left-hand boundary condition one then determines the value of $I$:

$$I^{-1} = \frac{1}{\beta_{0,1}} + \frac{1}{\beta_{1,2} f_1^{eq}} + \frac{1}{\beta_{2,3} f_2^{eq}} + \cdots \tag{15}$$

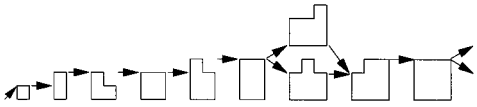

Fig. 2. The lowest-energy nucleation path for clusters with less than 10 particles. Note branching starting from $n = 6$. In the electric analogy clusters are "junctions" while connecting arrows are "resistors."

which, with somewhat different notations, can be traced to the work of Farkas.[5] The sum rapidly converges beyond the critical size $n_*$, where the equilibrium distribution $f_n^{eq}$ starts to increase.

General properties of the time-dependent Becker–Döring equations at large times are considered in ref. 32. For intermediate times, which are smaller than the lifetime of a metastable state, a matched asymptotic transient solution also can be constructed,[33] which allows one to trace the establishment of the steady-state regime (see also a more recent ref. 34). The multidimensional version of Eq. (14) described in the next section, however, is much more complex, and at the moment only steady-state solutions will be discussed.

A succession of the lowest energy configurations for the present problem is shown in Fig. 2. For larger supersaturations $S > 1/4$, when the critical size falls into the nonbranching part of the path, the conventional approach should provide an excellent approximation at small temperatures, provided one uses exact, rather than phenomenological[5] expressions for $f_n^{eq}$. For $S < 1/4$, however, the critical size falls into the branching part of the nucleation path. That means that several distinct shapes with the same $n$ should be considered, which requires a generalization of Eqs. (14).

### 3.2. Generalized Becker–Döring Equations

For each class $k \geqslant 1$ one can define the "incoming" and "outgoing" fluxes, $I_k^+$ and $I_k^-$, respectively:

$$I_k^+ = \sum_i \{\beta_{i,k} f_i - \alpha_{i,k} f_k\}$$
$$I_k^- = \sum_i \{\beta_{k,i} f_k - \alpha_{k,i} f_i\} \tag{16}$$

Summation runs over all classes with either $n(i) = n(k) - 1$ for the incoming fluxes, or with $n(i) = n(k) + 1$ for the outgoing fluxes. The time-dependence of cluster densities is then given by

$$\frac{df_k}{dt} = I_k^+ - I_k^- \tag{17}$$

These equations are valid as long as the fraction of the lattice sites occupied by the gas particles is small, i.e.,

$$\sum_k n(k)\, f_k \ll 1 \tag{18}$$

Violation of the above inequality could mean non-negligible effects of cluster-cluster interactions, which are not included in Eqs. (16) and (17).

With restrictions imposed by Eq. (18), the left-hand boundary condition is $f_0 = 1$. This is similar to conventional picture since there is no branching in that part of the nucleation path. The right-hand boundary conditions can be taken as $f_k \to 0$ for $n(k) \to \infty$. One expects that, asymptotically, the nucleation rate will be not too sensitive to the precise location of the absorbing boundary (for example, one could place it at some large, but finite $n_{\mathrm{up}}$), although an explicit demonstration of this insensitivity could be extremely challenging.

With the above selection of boundary conditions, one expects the existence of a steady-state solution, similarly to the Becker–Döring case.[32] Physically, such a solution makes sense as long as the inequality (18) holds, which implies exponentially weak limitations on time for an exponentially small nucleation rate.

To strengthen connection with the conventional picture, one can introduce a total number of clusters with $n$ particles, $F_n = \sum_k f_k$ (where summation is over all $k$ with $n(k) = n$) and a similar integral flux $J_n = \sum_k I_k^+$. From Eqs. (16) and (17) one obtains

$$\frac{dF_n}{dt} = J_n - J_{n+1} \tag{19}$$

The steady-state nucleation rate $I$ is the integral flux $J_n$ at any size. Otherwise, similarity with Eq. (14) is formal since the fluxes $J_n$ cannot be expressed through $F_n$ and $F_{n-1}$.

Once Eqs. (17) are treated as exact ones (i.e., the inequality (18) is disregarded and the boundary conditions are fixed), one does not expect any dramatic modifications in the solution beyond the original metastable

domain $0 < S < 1$. In particular, at $T > 0$ the solution should be a continuous function of $S$ at $S = 1$, and lead to a finite value of $I \to \beta_{0,1}$ for $S \to \infty$. The physical interpretation, of course, is very different since for $S > 1$ there is no barrier to nucleation and, rather than being a "nucleation rate," $I$ has the meaning of a rate with which particles enter the system. If one does invoke the inequality (18), the duration of such a solution becomes extremely short, for which reason the region $S > 1$ will be only of formal interest.

### 3.3. Electric Analogy

Consider Fig. 2 as a conducting path with classes being treated as electric junctions with voltages $V_k = f_k / f_k^{eq}$. Arrows which connect two classes $i$ and $k$ are "resistors" $R_{ik}$. If, for $i < k$ and $n(i) = n(k) - 1$, one defines

$$R_{ik} = 1 / \beta_{i,k} f_i^{eq} \tag{20}$$

then the partial fluxes $j_{ik} = \beta_{i,k} f_i - \alpha_{i,k} f_k$ can be treated as "currents"

$$j_{ik} = (V_i - V_k) / R_{ik} \tag{21}$$

This is the "Ohms law." The incoming and the outgoing fluxes for a class $k$ are given, respectively, by $I_k^+ = \sum_i j_{ik}$ and $I_k^- = \sum_i j_{ki}$. The steady state condition for Eq. (17), $I_k^+ = I_k^-$, is then the "junction rule."

Since the total voltage difference in the circuit is $V_0 = 1$, the total current $I$, which is the nucleation rate, is the inverse of the equivalent resistance. For a non-branching path, resistances are in series and just add up, which leads to Eq. (15). For branching, "Kirchoffs equations" are to be solved. Solution can be quite elaborate if all configurations are taken into account, and can be completed only for sufficiently large supersaturations (relatively small $n_{up}$).[24] In the lowest energy description, however, one has to deal only with additional simple series-parallel connections as in Fig. 2. Such connections can be be replaced by single branches with known equivalent resistance, restoring the one-dimensional structure of the problem.

## 4. THE PRE-EXPONENTIAL, AND THE LIMIT $T \to 0$

Following ref. 24 let us define the pre-exponential $A$ from the known zero-$T$ barrier, and from the nucleation rate $I$, which is yet to be calculated:

$$I^{-1} = A \exp\{W_* / T\} \tag{22}$$

In the metastable region $0 < S < 1$ the barrier $W_*$ follows from Eq. (8) with $m = m_*$ and is equivalent to the one obtained by Neves and Schonmann.[18] Formally, one can also include the region $S > 1$ by defining here the barrier as zero, so that the preexponential coincides with the inverse of the "rate" $I$.

### 4.1. Lattice Gas Dynamics

For $S > 1/4$, when the critical size falls into the non-branching part of Fig. 2, Eq. (15) can be applied directly. For non-integer $1/2S$ only the dominant term in the series, corresponding to the highest primary maximum ("the largest resistance") survives the limit $T \to 0$. This gives

$$A_0 = (w_{n_*} \beta_{n_*, n_*+1})^{-1}, \qquad n_* = 0, 1, 3 \tag{23}$$

I.e., $A_0 = 1/4$ for $1/4 < S < 1$, $S \neq 1/2$, and formally $A_0$ is 1 for $S > 1$ in accord with ref. 24.

For smaller $S \leqslant 1/4$, when $n_*$ falls into the branching part of the nucleation path, consider first a group of primary classes $k$ with the same $n(k) = n_p$ (e.g., the two 7-particle clusters in Fig. 2). From the left, each primary class is connected to the same $m$ by $(m+1)$ rectangle with $m = [\sqrt{n_p} - 1]$. The connecting "resistances," however, are negligible for $S < 1/2$ compared to the resistances from the right discussed below. (Thus, every primary class in this group has an identical "voltage" in the electric analogy). From the right, each of the primary classes $k$ is connected to some non-extremal class $i$ which has the shape of the aforementioned rectangle with two additional neighboring particles on the longer side (e.g, the 8-particle cluster in Fig. 2). Connecting resistances are given by

$$R_{ki} = \exp\{W_{n_p}/T\} / \beta_{k,i} w_k \tag{24}$$

where the exponential term is identical for all $k$ in the group. Resistances to the right of class $i$ are negligible, which means that all resistances given by Eqs. (24) are "in parallel." Thus, one has to add the inverses of $R_{ki}$ to get the inverse of the equivalent resistance, $R_{n_p}^{-1} = \exp\{-W_{n_p}/T\} \sum_{k,i} \beta_{k,i} w_k$ (summation is over all $k, i$ with $n(k) = n(i) - 1 = n_p$). The actual calculations are straightforward since $\beta_{k,i}$ can only have the value of 1 for an $m$ by $(m+1)$ rectangle with an extra particle near the corner of a longer side, or the value of 2 for any other location of the extra particle on that side. The value of $w_k$ is 8 for all configurations, except for the single symmetric configuration for an odd $m+1$, with $w_k = 4$. The result is insensitive to the parity of $m$, and is given by

$$R_{n_p} = \exp\{W_{n_p}/T\}/8m, \qquad m = [\sqrt{n_p}\,] - 1 \tag{25}$$

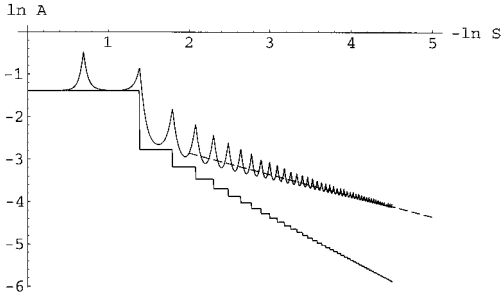


Fig. 3. Prefactor of the inverse nucleation rate, for $T = 0$ (the lower solid line), Eq. (23), and at $T > 0$, from Eq. (35), (upper solid line with $u = 10^{-7}$). The smooth asymptote—dashed line—is given by Eq. (45).

Contributions of secondary maxima are similar to the above, with $n_p$ replaced by $n_s$ and $m$ in the denominator replaced by $m-1$.

In the limit $T \to 0$ the equivalent resistance with $n_p = n_*$ dominates, giving the inverse of the nucleation rate. Since the corresponding value of $W_{n_p}$ coincides with the barrier $W_*$, the preexponential is

$$A_0 = 1/8m_* \tag{26}$$

This is valid for $m_* \geqslant 2$, with non-integer $1/2S$. The value of $A_0$ is shown by the lower line in Fig. 3.

Consider now an integer $1/2S$, which coincides either with $m_*$ or with $m_* - 1$, depending on the direction from which the integer number is approached. Here another primary and a neighboring secondary maxima will provide comparable contributions, leading to a sharp increase in the value of $A_0$. Specifically for $1/2S = m_* + 0$, the two additional maxima lead to identical equivalent resistances of $\exp\{W_*/T\}/8(m_* - 1)$, which are in series with the one in Eq. (25) evaluated at $n_p = n_*$. The preexponential is thus given by $1/4(m_* - 1) + 1/8m_*$. Replacing $m_*$ by $1/2S$ (which makes the result insensitive to the direction the integer limit is taken), one obtains

$$A_0^{\text{peak}}(S) = \frac{S(3-2S)}{4(1-2S)}, \qquad 1/2S = 3, 4, \ldots \tag{27}$$

For $S \to 0$ this is three times larger than $A_0$ in Eq. (26). Special values of $A_0^{\text{peak}}$ at $S = 1$, $1/2$, and $1/4$ are given, respectively by $5/4$, $5/8$, and $7/16$. One should keep in mind, however, that the peak at $S = 1/2$ will be modified by higher-energy nucleation paths, and is lower by about 50%, as follows from comparison with ref. 24–see also the Appendix below.

Although the peaks have a finite height, they will have a zero width at $T = 0$, for which reason they are not shown in the corresponding part of Fig. 3. Their contribution becomes important for finite $T$, as will be described later in the paper.

### 4.2. Glauber Dynamics

Let us introduce dimensionless variables

$$u = \mathrm{e}^{-\phi/T}, \qquad \delta = \mathrm{e}^{2\phi S/T} \tag{28}$$

to characterize the dependence on temperature and supersaturation, respectively. (In view of traditional applications of Glauber dynamics to the Ising model simulations, note that $u$ is the standard low-temperature expansion parameter for that model.[26] Futhermore, if in the Ising model the spin-spin interaction energy has the values of $\pm \mathrm{J}$, and the energy of a single spin in external field is $\pm \mathrm{H}$, equivalence with lattice gas is achieved with $\mathrm{J} = \phi/4$ and $\mathrm{H} = \phi S$).

Applying Eq. (13), one finds two general types of correcting factors

$$\beta^G_{i,k} = \frac{\beta_{i,k}}{1 + 1/\delta} \tag{29}$$

for transition to an non-extremal and

$$\beta^G_{i,k} = \frac{\beta_{i,k}}{1 + 1/u\delta} \tag{30}$$

for transition to an extremal class. A special case is

$$\beta^G_{0,1} = \frac{\beta_{0,1}}{1 + 1/u^2\delta} \tag{31}$$

At $T \to 0$ switching to Glauber dynamics mostly affects transition rates to extremal classes.

The nucleation path is similar to Fig. 2. However, now the resistors entering the extremal junctions either from left or from right will have comparable input. In the non-branching part one thus has

$$A^G_0 = 1/w_{n_*-1}\beta_{n_*-1,n_*} + 1/w_{n_*}\beta_{n_*,n_*+1}, \qquad n_* = 1, 3 \tag{32}$$

This gives for the preexponential, respectively, $5/4$ at $1 > S > 1/2$ and $3/8$ at $1/2 > S > 1/4$, in accord with ref. 20. For $S > 1$ one has $\beta^G_{0,1} = \beta_{0,1}$ and,

similarly to the lattice gas case, only one term contributing the the overal resistance, with the same result $A_0^G = 1$.

The easiest way to visualize calculations for the branching path, is to remove the degeneracy of an individual extremal class $k$ by breaking it into $w_k$ identical replicas. Each replica will be connected by an exactly one link ("resistor") to a lower non-extremal class and by one link to a higher class. After adding together the two associated resistors (which are in series to each other) for each of the replicas, one recovers $w_k$ parallel connections. Further treatment becomes quite similar to the lattice gas dynamics of the previous section. For non-integer $1/2S$ one obtains

$$A_0^G = \frac{3}{8m_* + 4}, \qquad m_* \geqslant 2 \tag{33}$$

Compared to ref. 21, the above equation (which is also valid for Metropolis dynamics) has an extra term "$+4$" in the denominator.

For integer $1/2S$ there is a simultaneous contribution of two primary and one secondary equivalent extremal resistances. Adding to $A_0^G$ in Eq. (33) twice that term with $m_*$ replaced by $m_* - 1$ (similarly to lattice gas dynamics), and substituting $1/2S$ for $m_*$ in the answer, one obtains

$$A_{0,G}^{\text{peak}}(S) = \frac{3S(3+S)}{4(1-S^2)}, \qquad 1/2S = 3, 4, \ldots \tag{34}$$

Again, for $S \to 0$ peaks are three times higher than non-special neighboring values of $A_0^G$. At $S = 1$, $1/2$ and $1/4$ the general pattern is not followed, and one has for the peak values of the prefactor, respectively, $9/4$, 2 and $31/40$. However, similarly to the lattice gas case, the second peak can be lower than 2 due to the contribution of higher-energy nucleation paths. Indeed, at $S = 1/2$ simulations[22, 25] indicate a value of the preexponential which is smaller by 10–15%. The peak at $S = 1/2$ is further reduced if Metropolis dynamics is considered instead of Glaubers, having a value of $13/8$ in the lowest energy path approximation. The peak at $S = 1$ will completely disappear for Metropolis dynamics. Other peaks will remain unchanged.

## 5. EXTRAPOLATION TO $T > 0$

In the present section the lowest energy nucleation path will be used to estimate the nucleation rate at small finite $T$. In doing so, one should keep in mind the potential contribution of the neglected higher-energy paths, and the question of the magnitude of those contributions remains open,

(see also the Discussion section below). Since those paths are "in parallel" to the nucleation path considered, they will all act in the direction of reducing the "equivalent resistance," sic. increasing the nucleation rate. Thus, the results obtained from the lowest-energy path should be treated as the lower bound for the nucleation rate or, equivalently, as the upper bound for the preexponential.

### 5.1. Lattice Gas Dynamics

In the previous section the problem has been reduced to a one-dimensional chain of equivalent resistances which connect the primary and secondary junctions. Only one dominant resistor (or at most three of them for integer $1/2S$) contributed in the limit $T \to 0$. The straightforward way to extrapolate the treatment to finite $T$ would be to use the sum of those equivalent resistances, which leads to an infinite series in powers of $u$ (for a fixed $\delta$), as discussed below. At non-zero $T$, however, one first needs to justify the neglect of all resistances which do not emerge from one of the extremal classes.

Consider Fig. 1. Note that for $n_p$ or $n_s$ reasonably close to $n_*$, the corresponding value of $W_{n_p}$ or $W_{n_s}$ can differ from $W_*$ by an arbitrarily small number if $S$ is small. This justifies inclusion of a large number of terms in the series expansion below. On the other hand, the non-extremal values of $W$ in Fig. 1 are separated from $W_*$ by a finite gap of at least $\phi(1-2S)$. The latter corresponds to a compact cluster with $n_* - 1$ particles; all other non-extremal configurations will have a larger separation from $W_*$. In the electric analogy, such configurations lead to resistances which are asymptotically small compared to the dominant resistance, and which are "in series" to it. Thus, contribution of such terms can be ignored for small $S$. When $S$ approaches or exceeds $1/2$, the gap disappears, but for $n \leqslant 3$ all resistors are "extremal" (see Fig. 2) and are taken into account anyway.

Thus, one still can consider only those equivalent resistances which can potentially contribute at $T = 0$, with unchanged individual values. The main difference is that at $T > 0$ the total resistance of the resulting one-dimensional chain will be determined by all resistors, and not only by the dominant one. This total resistance, which is the inverse of the nucleation rate $I$, is just the sum of individual contributions

$$I^{-1} = \sum_{m=1}^{\infty} \frac{u^{-\kappa_p(m,S)} + u^{-\kappa_s(m+1,S)}}{8m} + \Delta_0 \tag{35}$$

Here $\kappa_p = W_{n_p}/\phi$ and $\kappa_s = W_{n_s}/\phi$ are, respectively, the dimensionless "primary" and "secondary" energies, with $n_p$ and $n_s$ related to $m$ by Eqs. (8)

and (9). $\Delta_0$ corrects for contributions of small clusters which do not follow the general pattern:

$$\Delta_0 = 1 + \frac{1}{4u^2\delta} + \frac{1}{8u^3\delta^2} + \frac{1}{8u^4\delta^3} \tag{36}$$

(these corrections, however, are negligible for small supersaturations with $m_* \geqslant 2$). The pre-exponential $A$ is obtained by multiplying Eq. (35) by $u^{W_*/\phi}$, and is shown in Fig. 3.

In a general case, Eq. (35) determines a rather complex function of $u$ and $\delta$. Consider, however, $u \to 0$ with a *finite* $\delta$, which corresponds to a scaling limit $S, T \to 0$ with $S/T = \text{const}$. Here, the dependences on $S$ and $S/T$ factor, although the latter still will be determined by a special function.

Contributions of primary and secondary maxima can be evaluated separately. Introducing

$$a = m_* - 1/2S + 1/2 \tag{37}$$

with $|a| \leqslant 1/2$, one obtains the exponents in the expansion (35)

$$W_*/\phi - \kappa_p(m, S) = 2S(l^2 + 2la), \qquad l \equiv m - m_* \tag{38}$$

and

$$W_*/\phi - \kappa_s(m, S) = 2S(l^2 + (2l-1)(a-1/2)) \tag{39}$$

For the primary contribution this gives

$$A_p = \frac{1}{8} \sum_{l=1-m_*}^{\infty} \frac{1}{m_* + l} \left(\frac{1}{\delta}\right)^{l^2+2la} \tag{40}$$

For $m_* \gg 1$ the lower summation limit can be replaced by $-\infty$, while $l$ in the denominator can be neglected compared to $m_*$. The remaining series leads to an elliptic theta function $\theta_3(x, y)$[35] with one imaginary argument

$$A_p = B_p/8m_*, \qquad B_p = \theta_3\left(ia \ln \delta, \frac{1}{\delta}\right) \tag{41}$$

Similarly, for the contribution of secondary maxima, one obtains

$$A_s = B_s/8m_*, \qquad B_s = \theta_3\left(i\left(a - \frac{1}{2}\right) \ln \delta, \frac{1}{\delta}\right) \delta^{a-1/2} \tag{42}$$

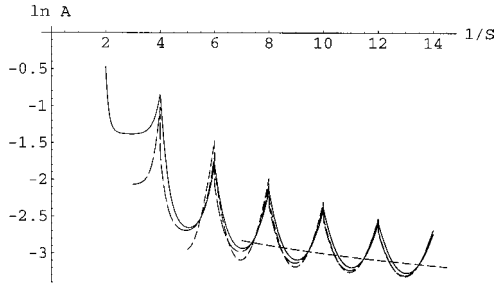


Fig. 4. Approximations to the prefactor at small $S$. Solid line and the monotonic dashed line are, respectively, the full expression [from Eq. (35)] and the smooth asymptote for $u = 10^{-7}$, same as in Fig. 3. The elliptic function approximation, Eq. (43), is shown by a longer-dash line, starting from $1/S = 3$. The $S \ll T/\phi$ asymptote, Eq. (44), is shown by a shorter-dash line starting from $1/S = 5$.

Thus, the total pre-exponential is given by

$$A = A_0(B_p + B_s) \tag{43}$$

Strictly speaking, within the accuracy of the treatment $A_0$ from Eq. (23) should be replaced by its continuous version, $\tilde{A}_0 = S/4$, but it helps to make obvious the connection with the zero-temperature limit. For $T \to 0$ one has, respectively, $B_p^0 = 1$, $B_s^0 = 0$ for non-integer $1/2S$, and $B_p^0 = 2$, $B_s^0 = 1$ for integer $1/2S$, so that in this limit Eq. (43) is consistent in with Section 4 for any small $S$.

Equation (43), together with its counterpart for Glauber dynamics described in the next section, are the main results of the present paper. For small supersaturations, Eq. (43) provides an asymptotically accurate approximation to the general expression (see Fig. 4). For a fixed supersaturation, the temperature dependence is smooth. Alternatively, for a fixed $T$ the $S$-dependence has a saw-tooth structure, as in Fig. 4.

The general expression has elementary asymptotes for $\delta \to 1$ (small supersaturation) and $\delta \to 0$ (small temperature), respectively. The former case corresponds to a large number of terms contributing to the sums in Eq. (35), which can be replaced by integrals. This gives

$$A \approx A_0 \sqrt{\frac{\pi}{\ln \delta}}\,(\delta^{a^2} + \delta^{a^2 - 1/4}), \qquad S \ll T/\phi \tag{44}$$

Peaks in Fig. 4 are described by this approximation, although there are small discontinuities which are not seen in the scale of the figure (discontinuities are removed if the smooth version $\tilde{A}_0 = S/4$ is used instead

of $A_0$—see the example of the Glauber dynamics below—which otherwise practically does not affect the accuracy of the approximation). In the original variables one has an asymptotic dependence

$$A \sim \frac{1}{4}\sqrt{\frac{\pi ST}{2\phi}} \tag{45}$$

for the "smooth" part of the pre-exponential. Small scale modulations appear if the above expression is multiplied by $1+(2a^2-1/4)\,\phi S/T$. Local maxima (peaks) are located at $a=\pm 1/2$, while $a=0$, approximately, locates the minima of modulations.

In the "cold" limit $\delta \gg 1$ the maximal term in Eq. (35) is dominant. However, there are four additional terms (two primary and two secondary maxima) which potentially give a comparable contribution for special values of the supersaturation. In order to account for such cases, one needs a 5-term approximation

$$A_5 = A_0 + \frac{\delta^{a-1/2}+\delta^{2a-1}}{8(m_*-1)} + \frac{\delta^{-a-1/2}}{8m_*} + \frac{\delta^{-2a-1}}{8(m_*+1)}, \qquad m_* \geqslant 3 \tag{46}$$

One can check that this expression is continuous—the discontinuities in $a$ and $m_*$ compensate each other. This is an accurate approximation for finite $S$ (which, in the region of its applicability, would practically blend in with the solid curve in the scale of Fig. 4), and which leads to a correct zero-temperature limit. It gives, however, a typical $A \sim S$ dependence for $S \to 0$ and finite $T$, instead of the square root asymptote, as in Eq. (45).

Deviation from the zero-$T$ limit, approximately, is the smallest at the midpoints between the peaks, at odd $1/S$, where it scales as $\delta^{-1/2}$. Deviation increases towards even $1/S$, where it scales as $\delta^{|a|-1/2}$. This is in qualitative agreement with conclusions based on simulations for Glauber dynamics,[25] although remarkably, directly at even $1/S$ deviation from the limit $T=0$ is the smallest, as shown below.

Peaks at integer $1/2S$ are given by

$$A^{\text{peak}} = A_0^{\text{peak}} + \frac{1}{8m_*\delta} + \frac{1}{8(m_*+1)\,\delta^2} \tag{47}$$

Note that the finite-$T$ corrections are smaller (have a larger negative power of $\delta$) compared to those at non-special values. In other words, as temperature is lowered, the limiting values of $A$ in a given finite interval of $1/S$ (fixed $m_*$) are first approached at even $1/S$, at the peaks, then at odd $1/S$, and then in the rest of the interval.

The width of a peak is given by $T/(4\phi S)$. This should be compared to the distance between peaks, which is $S^2/2$ for $S \ll 1$. Thus, already at a rather low temperature $T/\phi > 2S^3$, peaks are broad enough to dominate the pre-exponential.

### 5.2. Glauber Kinetics

As shown in Section 4, in the Glauber case one has to consider *two* groups of "resistors" which are connected to each extremal junction, respectively from left and from right. According to Eqs. (29)–(31) these two groups have a different temperature dependence, which somewhat complicates the situation compared to lattice gas dynamics. Nevertheless, after all resistor spanning a group of extremal junctions with a given number of particles, are replaced by a single equivalent resistor (where relative contributions from left and from right will be skewed compared to $T = 0$), the problem is again reduced to an effectively one-dimensional one. Adding the resulting resistances gives the total equivalent resistance of the chain, which is the inverse nucleation rate:

$$I_G^{-1} = \sum_{m=2}^{\infty} \left( g(m, \delta)\, u^{-\kappa_p(m, S)} + g(m-1, \delta)\, u^{-\kappa_s(m, S)} \right) + \Delta_0^G \tag{48}$$

with

$$g(m, \delta) = \left(3 + \frac{1}{\delta}\right)\left(8m + \frac{4}{1 + 1/2\delta}\right)^{-1} \tag{49}$$

and

$$\Delta_0^G = 1 + \frac{5}{4u^2\delta} + \frac{3}{8u^3\delta^2} + \frac{3}{8u^4\delta^3} + \frac{1}{4u^4\delta^4} \tag{50}$$

The latter correction appears due to violation of the general pattern for smaller clusters, and can be traced to the non-branching part of Fig. 2.

Once the nucleation rate is known, the preexponential follows from Eq. (22). Qualitatively, the structure of the preexponential is very similar to the one from lattice gas dynamics, which is shown in Fig. 3, although the numerical values in the Glauber case are higher, and at $T = 0$ there is an additional discontinuity at $S = 1/2$.[20] In the region $1/4 \lesssim S \lesssim 1/2$ and small temperatures, Eq. (48) is in reasonable agreement with corresponding simulation data of ref. 25, although the latter are slightly lower near $S = 1/4$ and $S = 1/2$ due to contributions of higher-energy nucleation

paths. Correction for such paths and a more detailed comparison will be a subject of a separate study.[36]

For small supersaturation the $\Delta$-term does not contribute, while summation of the series can be expressed in terms of elliptic theta-functions, similarly to the case of lattice-gas dynamics. One thus obtains

$$A^G \approx \tilde{A}_0^G(1+1/3\delta)(B_p+B_s), \qquad \tilde{A}_0^G = 3S/4(S+1) \tag{51}$$

where $\tilde{A}_0^G$ is the smooth version of the zero-temperature limit, Eq. (33) with $m_*$ replaced by $1/2S$, while $B_p$ and $B_s$ are the same as defined in Eqs. (41) and (42).

Similarities with Eq. (43) allow one to use almost verbatim the approximations of the previous section. In particular, for $S \ll T/\phi$ one has an asymptotic dependence

$$A^G \sim \sqrt{\frac{\pi ST}{2\phi}} \tag{52}$$

which is exactly four times larger than for lattice gas dynamics.

At low-temperatures a five-term approximation can be constructed similarly to Eq. (46) by selecting the leading primary term in Eq. (48) (the one with $m = m_*$), and adding two primary and two secondary terms with $m = m_* \pm 1$. For $m_* \geqslant 3$ one has

$$\begin{aligned} A_5^G = {} & g(m_*, \delta)(1+\delta^{-1/2-a}) + g(m_*-1, \delta)(\delta^{a-1/2}+\delta^{2a-1}) \\ & + g(m_*+1, \delta)\,\delta^{-1-2a} \end{aligned} \tag{53}$$

Compared to lattice gas dynamics, there is an additional dependence on $\delta$ through the coefficients $g$. For large $\delta$, however, such corrections are small as $1/\delta$ and, qualitatively, conclusions about the width of the peaks and their sensitivity to temperature remain unchanged.

In case of Metropolis dynamics (MD) there are a few modest modifications. The small-cluster correction is given by

$$\Delta_0^M = \max(1, 1/u^2\delta) + \max(1, 1/u\delta)(1/4u^2\delta + 1/8u^3\delta^2) + 1/4u^4\delta^3 \tag{54}$$

This determines the inverse of the nucleation rate for $S \geqslant 1/2$. For smaller $S$ the nucleation rate appears to be an analytic function of $S$ (since there are no near-idle transitions with $W_i \approx W_k$ where rates in MD can become non-analytic). An expansion similar to the one in Eq. (48) can be used, but with the zero-temperature values of the coefficients, $g(m, 0)$ which are not renormalized with temperature, in contrast to Glauber dynamics (in this

sense, the MD is simpler). With such modifications, Eq. (53) for the low-temperature preexponential also can be used for MD, and the general Eq. (51) is valid once the term $1/3\delta$ is dropped. The small-$S$ asymptote in Eq. (52) is multiplied by $3/4$ in case of MD.

## 6. SUMMARY OF THE RESULTS AND OPEN QUESTIONS

The inverse nucleation rates along the lowest-energy path are given by expansions (35) and (48) for the lattice gas and Glauber dynamics, respectively. For non-special values of $S$ both expansion have a single maximum term which determines the exponential part of the nucleation rate (equivalent to the one of ref. 18), as well as the zero-temperature limit of the pre-exponential. Special cases are integer $1/2S$, when at least three terms have comparable contributions, which modifies the preexponential. The number of contributing terms increases with temperature. For small $S \ll 1$ general expansions can be evaluated in terms of elliptic theta-functions—see Eqs. (43) and (51). For $S \gg T/\phi$ and $S \ll T/\phi$ further simplifications are possible which lead to elementary functions.

When plotted as functions of inverse supersaturation, the preexponentials for both dynamics will have a typical saw-tooth structure, as the upper line in Fig. 3. This notably differs from the zero-temperature limit (lower line in that figure), even at rather low temperatures. Deviation increases at smaller supersaturations, and a temperature which is *cubic* in $S$ is required for the limit to become apparent.

Sharp peaks observed in ref. 24 at relatively large $S$, are confirmed at any integer $1/2S$ both for lattice gas and Glauber dynamics. For both dynamics, at $T = 0$ and $S \ll 1$ peaks are three times higher than the neighboring non-special values. For finite $T$, however, the relative amplitude of those peaks linearly diminishes for small $S$.

The electric analogy allows one to visualize the nucleation flux as a current through a branching network. The nucleation rate is then the inverse of the equivalent resistance of the network. The conventional description of nucleation as a one-dimensional random walk,[5] can be described in terms of a simple "Ohms law." Branching paths (which appear even at $T = 0$), generally speaking, require more elaborate "Kirchoffs equations." It turns out, however, that only certain extremal parts of the network provide the dominant resistance at small $T$, and examining the parallel-series connections in the vicinity of those junctions allows one to reduce the problem to a one-dimensional chain of resistors, and write down an explicit solution.

Modulations of the preexponential (or strong oscillations in the imaginary part of the free energy observed in transfer matrix studies[16, 37])

should not obscure the fact that the nucleation rate is expected to remain a monotonic function of the supersaturation for a fixed temperature. In terms of the electric analogy, increasing of $S$ leads to the decrease of every one of the resistances which enters into the network, and one can anticipate that its equivalent resistance will also decrease. This makes the nucleation rate a monotonically increasing function of $S$ for all $S$, and for all types of the dynamics considered. Available simulations for $S \gtrsim 1/6$ with Glauber dynamics[25] seem to confirm this conclusion.

Comparing the lattice gas and the Glauber dynamics, one notes that despite qualitative similarities, Glauber dynamics is more sophisticated in the nucleation context in that the gain coefficient $\beta_{i,k}$ rapidly oscillates with the number of particles in a cluster, $n$, becoming very small for $n$ immediately preceding an "extremal" value. This is different from the lattice gas dynamics (and from the conventional nucleation approaches[5]) where gain only moderately changes with size. Technically, complications due to Glauber kinetics result in an additional group of "resistors" which enter each extremal junction. The difference becomes most obvious in the nonbranching part of the nucleation path of Fig. 2. For both dynamics the classical-type expression, Eq. (15) is valid here, but only in the lattice gas case, generally there will be a *single* dominant term (determined by the minimum $f_n^{eq}$) in the limit $T \to 0$. The resulting preexponential—Eq. (23)—thus bears certain similarities with the early guess by Volmer and Weber.[5] In the Glauber case, on the other hand, there will be at least two comparable terms—see Eq. (32)—which has no analogs in ref. 5. In that sense, the lattice gas kinetics where links with conventional treatments are obvious, can have an advantage, although it is likely to remain open to dispute which of the dynamics better mimics a given physical system.

The lowest energy nucleation path considered in the present study provides a bare, backbone contribution to the nucleation rate. This still can be increased by higher-energy nucleation paths, lowering the preexponential. At special values of supersaturation, especially at $S = 1/2$, this effect can be quite noticeable even at $T \to 0$. For Glauber and lattice gas dynamics, respectively, this conclusion follows from comparison with data reported in refs. 22 and 24 which included higher-energy nucleation paths. The peak at $S = 1/4$, on the other hand is lowered by only a few percent, and elucidation of such questions will require a separate study.[36]

A related open question[38] is the connection with the macroscopic description of nucleation based on the so-called droplet model (DM). In the DM the shape of a nucleus (which is anisotropic at low $T$) and the barrier to nucleation are determined from the Wulff droplet construction. There are estimations of the preexponential in the higher-temperature region, which are supported by simulations,[15] but less is known about the

preexponential at small $T$. In terms of the present work, the macroscopic limit would be recovered for $S \to 0$ (with $n_* \to \infty$), with a finite $T$. The number of higher-energy paths in that limit, however, becomes unboundedly large, which can lead to a noticeable change in the preexponential despite the exponentially small individual contributions of such paths. In other words, the neglect of higher-energy paths restricts the present treatment to values of $S$ which are not exponentially small in temperature. This allows one to consider the small $S$, $T$ limit in the order $T \to 0$, $S \to 0$, but not in the opposite order $S \to 0$, $T \to 0$, which is required for the identification with the DM. At the same time, one notes that at finite fixed $T$ the present treatment provides an upper bound for the preexponential, which decays for small $S$, in clear contrast with the DM where the preexponential unboundedly *increases* as $S \to 0$. This could mean that the DM preexponential cannot be applied at low $T$, although due to the difference in nucleation barriers used in the DM and in the present study, direct comparison of preexponentials remains quite a non-trivial task.

## APPENDIX A: LOWERING OF PEAKS BY HIGHER-ENERGY PATHS

One could expect that the paths which involve non-compact cluster configurations will have a negligible contribution for $T \to 0$. This is generally true for non-special values of the supersaturation, but the situation is more subtle at near-integer values of $1/2S$. Here, the "dormant" compact configurations which are not connected directly to any of the other lowest energy configurations (and which are thus excluded from the main nucleation path considered), can turn important.

Consider, e.g., a small domain of $S$ around $1/2$, with $S > 1/2$ corresponding to $n_* = 1$ and $S < 1/2$ to $n_* = 3$. The corresponding segment of the main nucleation path in Fig. 2 connects the single-particle cluster, the dimer, the L-shaped—particle cluster and, neglecting the square which leads to a negligible "resistance," the 5 particle cluster. Individual resistances for each element of this path are given, respectively, by $R_{1,2} = 1/(4u^2\delta)$, $R_{2,3} = 1/(4u^3\delta^2)$ and $R_{3,5} = 1/(4u^4\delta^3)$. The resistor $R_{1,2}$ dominates for $u\delta \gg 1$ (which is $S > 1/2$), and the resistor $R_{3,5}$ dominates for $u\delta \ll 1$. All of the resistors have a comparable contribution for $\delta \sim 1/u$, which is at $S = 1/2$. Now consider one of the additional paths which links the the dimer and the 5 particle cluster of Fig. 2. This path contains the "minus"-shaped 3-particle cluster, and one of the higher-energy shapes of the 4-particle cluster, which are not shown in that figure. (Possible links with the L-shaped 3-particle cluster are not important for the qualitative discussion). Without numerical constants, the resistances involved in the additional path are, respectively, $1/u^3\delta^2$, $1/u^4\delta^3$, $1/u^5\delta^4$. The overall resistance of this

path is asymptotically larger than $R_{3,5}$ for $S < 1/2$ or than $R_{1,2}$ for $S > 1/2$, respectively. Generally, this justifies the neglect of the additional path at $T \to 0$. On the other hand, for $S = 1/2$ this path provides a comparable contribution. The actual expression is rather elaborate[24] since the aforementioned extra link to the L-shaped 3-particle cluster leads to a "Wheatstone bridge" (in electric terminology) with notoriously cumbersome equivalent resistance.

## ACKNOWLEDGMENTS

I am grateful to O. Penrose for detailed critical comments on the manuscript, and to P. A. Rikvold and M. A. Novotny for useful remarks and correspondence.

## REFERENCES

1. F. F. Abraham, *Homogeneous Nucleation Theory* (Academic Press, New York, 1974).
2. A. A. Chernov, *Modern Crystallography III, Crystal Growth* (Springer, Berlin, 1984).
3. P. Debenedetti, *Metastable Liquids* (Princeton, New Jersey, 1996).
4. A. D. Linde, *Uspekhi Fisicheskih Nauk* **144**:177 (1984).
5. M. Volmer and A. Weber, *Z. Phys. Chem.* **119**:227 (1926); L. Farkas, *ibid.*, **125**:236 (1927); R. Becker and W. Döring, *Ann. Phys.* **24**:719 (1935); Ya. B. Zeldovich, *Acta Physicochim. (USSR)* **18**:1 (1943); J. Frenkel, *Kinetic Theory of Liquids* (Oxford University, Oxford, 1946).
6. J. Lothe and G. Pound, *J. Chem. Phys.* **36**:2080 (1962).
7. H. Reiss, J. L. Katz, and E. Cohen, *J. Chem. Phys.* **48**:5553 (1968).
8. C. Rottman and M. Wortis, *Phys. Rev. B* **24**:6274 (1981); R. K. P. Zia and J. E. Avron, *Phys. Rev. B* **25**:2042 (1982).
9. R. K. P. Zia, *J. Stat. Phys.* **45**:801 (1986); V. A. Shneidman and R. K. P. Zia, *Phys. Rev. B* **63**:085410 (2001).
10. M. E. Fisher, *Phys.* **3**:255 (1967).
11. J. S. Langer, *Ann. Phys. (N.Y.)* **65**:53 (1971).
12. N. J. Günther, D. A. Nicole, and D. J. Wallace, *J. Phys. A* **13**:1755 (1980).
13. J. D. Gunton, M. San Miguel, and P. S. Sahni, in *Phase Transitions and Critical Phenomena*, Vol. 8, C. Domb and J. L. Lebowitz, ed. (Academic, New York, 1983), p. 267.
14. E. Stoll, K. Binder, and T. Schneider, *Phys. Rev. B* **6**:2777 (1972); K. Binder and D. Stauffer, *Adv. Physics* **25**:343 (1976).
15. P. A. Rikvold, H. Tomita, S. Miyashita, and S. W. Sides, *Phys. Rev. E* **49**:5080 (1994).
16. C. C. Günther, P. A. Rikvold, and M. A. Novotny, *Phys. Rev. Lett.* **71**:3898 (1993); *Phys. A* **212**:194 (1994).
17. V. A. Shneidman, K. A. Jackson, and K. M. Beatty, *J. Chem. Phys.* **111**:6932 (1999).
18. E. J. Neves and R. H. Schonmann, *Commun. Math. Phys.* **137**:209 (1991).
19. R. Kotecky and E. Olivieri, *J. Stat. Phys.* **75**:409 (1994).
20. M. A. Novotny, Low-temperature metastable lifetimes of the square-lattice Ising ferromagnet, in *Springer Proc. in Physics, Vol. 82: Computer Simulation Studies in Condensed-Matter Physics IX*, D. P. Landau, K. K. Mon, and H.-B. Schüttler, eds. (Springer, Berlin, 1997), p. 182.

21. A. Bovier and F. Manzo, *J. Stat. Phys.* **107**:757 (2002).
22. K. Park and M. A. Novotny, *cond-mat/0109214* (2001).
23. M. A. Novotny, *cond-mat/0108429* (2001).
24. V. A. Shneidman and G. Nita, *Phys. Rev. Lett.* **89**:25701 (2002).
25. M. A. Novotny, *cond-mat/0204098* (2002).
26. R. J. Baxter. *Exactly Solved Models in Statistical Mechanics*, Chap. 1 (Academic Press, New York, 1982).
27. M. Kalos, J. L. Lebowitz, O. Penrose, and A. Sur, *J. Stat. Phys.* **18**:39 (1978).
28. O. Penrose and J. L. Lebowitz, in *Studies in Statistical Mechanics*, Vol. VII, Fluctuation Phenomena, E. Montrol and J. L. Lebowitz, eds. (North-Holland, Amsterdam, 1979); J. Ball, J. Carr, and O. Penrose, *Commun. Math. Phys.* **104**:657 (1986).
29. V. A. Shneidman, K. A. Jackson, and K. M. Beatty, *J. Cryst. Growth* **212**:564 (2000).
30. J. P. Marchand and P. A. Martin, *Phys. A* **127**:681 (1984).
31. Ph. A. Martin, *J. Stat. Phys.* **16**:149 (1977).
32. O. Penrose, *Commun. Math. Phys.* **124**:515 (1989).
33. V. A. Shneidman, *Sov. Phys. Tech. Phys.* **32**:76 (1987); *ibid.* **33**:1338 (1988).
34. V. A. Shneidman, *J. Chem. Phys.* **115**:8141 (2001).
35. M. Abramowitz and I. Stegun, *Handbook of Mathematical Functions* (Dover, New York, 1972).
36. V. A. Shneidman and G. M. Nita, in preparation.
37. S. B. Rutkevich, *J. Stat. Phys.* **104**:589 (2001).
38. P. A. Rikvold and M. A. Novotny, private communication.